



## Abstract

Aerosol radiative effects and thermodynamic responses over South Asia are examined with a version of the Weather Research and Forecasting model coupled with Chemistry (WRF-Chem) for March 2012. Model results of Aerosol Optical Depth (AOD) and extinction profiles are analyzed and compared to satellite retrievals and two ground-based lidars located in the northern India. The WRF-Chem model is found to underestimate the AOD during the simulated pre-monsoon month and about 83 % of the model low-bias is due to aerosol extinctions below  $\sim 2$  km. Doubling the calculated aerosol extinctions below 850 hPa generates much better agreement with the observed AOD and extinction profiles averaged over South Asia. To separate the effect of absorption and scattering properties, two runs were conducted: in one run (Case I), the calculated scattering and absorption coefficients were increased proportionally, while in the second run (Case II) only the calculated aerosol scattering coefficient was increased. With the same AOD and extinction profiles, the two runs produce significantly different radiative effects over land and oceans. On the regional mean basis, Case I generates 48 % more heating in the atmosphere and 21 % more dimming at the surface than Case II. Case I also produces stronger cooling responses over the land from the longwave radiation adjustment and boundary layer mixing. These rapid adjustments offset the stronger radiative heating in Case I and lead to an overall lower-troposphere cooling up to  $-0.7 \text{ K day}^{-1}$ , which is smaller than that in Case II. Over the ocean, direct radiative effects dominate the heating rate changes in the lower atmosphere lacking such surface and lower atmosphere adjustments due to fixed sea surface temperature, and the strongest atmospheric warming is obtained in Case I. Consequently, atmospheric dynamics (boundary layer heights and meridional circulation) and thermodynamic processes (water vapor and cloudiness) are shown to respond differently between Case I and Case II underlying the importance of determining the exact portion of scattering or absorbing aerosols that lead to the underestimation of aerosol optical depth in the model. In addition, the model results suggest that both direct radiative effect and rapid

## Radiative and thermodynamic responses to aerosol

Y. Feng et al.

Title Page

Abstract

Introduction

Conclusions

References

Tables

Figures



Back

Close

Full Screen / Esc

Printer-friendly Version

Interactive Discussion



thermodynamic responses need to be quantified for understanding aerosol radiative impacts.

## 1 Introduction

South Asia, including the Indian subcontinent and adjacent oceans, is a regional hotspot with high aerosol loadings (Ramanathan et al., 2001; Moorthy et al., 2013). Aerosols over this region are composed of locally emitted sulfate, black carbon (BC), and organic substances (mainly from industrial activities, transportation, residential, and agricultural burnings), as well as long-range transported desert dust and sea spray aerosols. These aerosols together induce a large negative radiative forcing at the top of the atmosphere (TOA) through direct scattering and absorption of incoming solar radiation. With year 2000 emissions, Chung et al. (2010) estimated the regional TOA aerosol forcing in South Asia at about  $-1.9 \text{ W m}^{-2}$ , which is larger by several factors than the present-day global mean direct forcing (Boucher et al., 2013). The overall aerosol cooling effect in response to negative TOA forcing is suggested to weaken the sea surface temperature gradient over the Indian Ocean and decelerate the monsoonal circulation and moisture transport (Ramanathan et al., 2005). Other studies show that local warming by BC in the upper troposphere intensifies vertical motion over land and modulates intraseasonal monsoon rainfall variations (Lau et al., 2006). Therefore, rapidly increased anthropogenic aerosol emissions in South Asia have been linked closely to observed changes in surface temperature and rainfall patterns in global climate simulations (Meehl et al., 2008; Lau et al., 2009; Wang et al., 2009; Bollasina et al., 2011; Ganguly et al., 2012).

For quantifying aerosol direct perturbations in the radiation budget, column-integrated aerosol optical depth (AOD) is often examined in global models, some of which include regional analysis over South Asia (Myhre et al., 2009, 2013; Shindell et al., 2013; Boucher et al., 2013; Pan et al., 2014), and in regional-scale models (Chung et al., 2010; Nair et al., 2012; Kumar et al., 2014). Besides AOD, aerosol single

## Radiative and thermodynamic responses to aerosol

Y. Feng et al.

Title Page

Abstract

Introduction

Conclusions

References

Tables

Figures



Back

Close

Full Screen / Esc

Printer-friendly Version

Interactive Discussion



**Radiative and  
thermodynamic  
responses to aerosol**

Y. Feng et al.

Title Page

Abstract

Introduction

Conclusions

References

Tables

Figures



Back

Close

Full Screen / Esc

Printer-friendly Version

Interactive Discussion



scattering albedo (SSA) has also been identified as a main source of uncertainty in estimates of aerosol direct forcing (McComiskey et al., 2008; Loeb and Su et al., 2010) and evaluated with observations. Most models underpredict aerosol abundances over South Asia vs. data from the ground-based Aerosol Robotic Network (AERONET) (Holben et al., 1998) or satellite-retrieved AOD observations such as the Moderate Resolution Imaging Spectroradiometer (MODIS) (e.g., Yu et al., 2003; Kinne et al., 2006; Koch et al., 2009; Ganguly et al., 2012). In addition, models also tend to underestimate aerosol absorption by over-estimating the SSA (Liu et al., 2012). Such low biases in aerosol optical properties might potentially affect model simulations of regional climatology and assessment of aerosol climate impacts over the South Asia region.

Vertical distribution of aerosols is another important parameter in determining aerosol-radiation interactions. When column AOD is constrained, uncertainties in aerosol vertical profiles can still contribute to significant uncertainties in the calculation of radiative forcing (Lohmann et al., 2001; Zarzycki and Bond, 2010; Ban-Weiss et al., 2011). The extent to which the aerosol profile impacts aerosol radiative effects depends on the presence of cloud, surface albedo, and SSA. Column and global aerosol and radiation models have been used to explore the sensitivity of aerosol direct radiative forcing to the vertical distribution of aerosols, especially absorbing aerosols, relative to clouds (Haywood and Shine, 1997; Liao and Seinfeld, 1998; Samset et al., 2013; Vuolo et al., 2014; Choi and Chung, 2014). However, compared to column AOD and SSA, aerosol vertical distributions are evaluated less frequently against observations, partly due to lack of observational data sets.

Aircraft profiling of aerosol concentrations from recent airborne experiments, such as the HIAPER Pole-to-Pole Observations (Schwarz et al., 2010) and the Arctic Research of the Composition of the Troposphere from Aircraft and Satellites (Jacob et al., 2010), provides high-quality data sets for model comparison (e.g., Koch et al., 2009; Liu et al., 2012). However, these data sets are usually available only for limited locations and time periods. In particular, few long-term aircraft surveys are available for South Asia, other than a few past field experiments such as the Maldives Autonomous Un-

**Radiative and  
thermodynamic  
responses to aerosol**

Y. Feng et al.

[Title Page](#)[Abstract](#)[Introduction](#)[Conclusions](#)[References](#)[Tables](#)[Figures](#)[Back](#)[Close](#)[Full Screen / Esc](#)[Printer-friendly Version](#)[Interactive Discussion](#)

manned Aerial Vehicle Campaign (Ramanathan et al., 2007) and the Integrated Campaign for Aerosol, Gases and Radiation Budget experiment (Satheesh et al., 2009). Satellite-retrieved aerosol extinction profiles providing wide coverage in space and time have been used increasingly for model evaluation. Using the Cloud-Aerosol Lidar and Infrared Pathfinder Satellite Observations (CALIPSO) lidar nighttime data at 532 nm in cloud-free conditions from June 2006 to November 2007, Yu et al. (2010) evaluated aerosol extinction profiles simulated by the Goddard Chemistry Aerosol Radiation Transport (GOCART) model and found substantial underestimation in the magnitude of aerosol extinctions over the Indian subcontinent. Similar analysis of all-sky CALIPSO nighttime data in the AeroCom (Aerosol Comparisons between Observations and Models) multi-model evaluation of the vertical distribution of aerosols (Koffi et al., 2012) found that 11 of the 12 AeroCom models underestimated the annual mean aerosol extinctions below 2 km over South Asia.

Although these model-data comparisons help to identify the biases in model simulations of aerosol extinction or concentration profiles, the resultant changes in atmospheric heating, dynamics, and cloud adjustments (the aerosol semi-direct effects) have yet to be investigated. Moreover, satellite retrievals of aerosol extinction profiles are also subject to uncertainties associated with cloud contamination, surface overlap correction, and daylight background noise. Observational studies have examined atmospheric heating rates extensively by using aerosol extinctions retrieved from ground-based or CALIPSO lidar instruments (Misra et al., 2012; Gautam et al., 2010; Kuhlmann and Quaas, 2010) and in situ aircraft data (Ramana et al., 2007; Satheesh et al., 2008). These studies directly provide observational constraints on the instantaneous atmospheric heating caused by aerosols, ranging from  $0.35$  to  $2 \text{ K day}^{-1}$ , in the South Asia region. On the other hand, observational methods face challenges in distinguishing the rapid adjustments in the atmosphere attributable to aerosols vs. other environmental influences.

In the present study, we examine the atmospheric radiative and thermodynamic responses to uncertainty associated with vertical distributions of aerosol extinction coeffi-

cient by correcting bias in model calculations with satellite and surface remote sensing data. This not only identifies discrepancies between the model-predicted and observed aerosol optical properties as a function of height, but it also demonstrates the potential importance of aerosol-related uncertainty for regional climate simulations. The regional Weather Research and Forecasting (WRF) model, coupled with a chemistry module (WRF-Chem), is used to simulate the pre-monsoon month of March 2012 over South Asia. The next section describes the regional climate model configurations and ground-based and satellite data sets available. Section 3 evaluates the modeled and observed AODs and aerosol profiles and discusses changes in the simulated radiative energy balance, surface temperature, lower-atmospheric heating rates, boundary layer (BL) height, large-scale circulation, and cloud occurrence, in response to optimized matching of aerosol extinction profiles to observations. The main findings of this study and implications for future work are summarized in Sect. 4.

## 2 Methodology

### 2.1 Model description

This study uses a version of the WRF-Chem 3.3 (Skamarock et al., 2008; Grell et al., 2005), coupled with the chemistry module MOZCART (Pfister et al., 2011), to simulate aerosol distributions, aerosol-radiation interactions, and regional meteorological fields. The default model simulations are performed for eight months from August 2011 to March 2012, the period when multi-instrumental aerosol observations were collected by the U.S. Department of Energy (DOE) Ganges Valley Aerosol Experiment (GVAX) at a mountain-top site, Nainital (29° N, 79° E, above sea level (a.s.l.) 1939 m), in northern India. The model domain is configured from 55 to 95° E and 0 to 36° N, with a horizontal grid spacing of ~ 12 km and 27 vertical layers. The MOZCART chemistry module (Kumar et al., 2014) includes the MOZART-4 gas-phase chemistry (Emmons et al., 2010) and the GOCART bulk aerosol scheme (Chin et al., 2002). MOZCART simulates ex-

## Radiative and thermodynamic responses to aerosol

Y. Feng et al.

Title Page

Abstract

Introduction

Conclusions

References

Tables

Figures



Back

Close

Full Screen / Esc

Printer-friendly Version

Interactive Discussion



ternally mixed aerosol species in transport including sulfate, BC, organic carbon (OC), dust (in 5 size bins with 0.5, 1.4, 2.4, 4.5, and 8  $\mu\text{m}$  effective radius) and sea salt (in 4 size bins with 0.3, 1.0, 3.2, and 7.5  $\mu\text{m}$  effective radius). This version of the WRF-Chem aerosol and chemistry modules has been used and evaluated in studying effects of dust aerosols on tropospheric chemistry during the pre-monsoon season in northern India (Kumar et al., 2014).

The anthropogenic emissions of gaseous species are derived from the Reanalysis of the Tropospheric Chemical Composition and Emissions Database for Global Atmospheric Research compiled for the year 2000. The default emissions of BC, OC, and  $\text{SO}_2$  are same as in the GOCART model for year 2006. Over India, emissions of BC, OC, and  $\text{SO}_2$  are replaced with year 2010 inventories available at resolutions of  $0.1^\circ \times 0.1^\circ$  for anthropogenic sources and  $0.5^\circ \times 0.5^\circ$  for biomass burning (Lu et al., 2011). The total emissions of BC and OC used in this study are about 1.12 and  $3.06 \text{ Ggyr}^{-1}$  over India, respectively, roughly 51 and 63% higher than those from the default GOCART global inventories (0.74 and  $1.88 \text{ Ggyr}^{-1}$ ). The compiled  $\text{SO}_2$  emissions of  $9.36 \text{ Ggyr}^{-1}$  are comparable to the GOCART emissions ( $10 \text{ Ggyr}^{-1}$ ). Additional sulfate emissions from waste and biofuel burning (Yevich and Logan, 2003) are also included (about  $0.21 \text{ Ggyr}^{-1}$ ). Dimethyl sulfide, dust, and sea salt emissions are calculated online as for the GOCART model (Ginoux et al., 2001; Chin et al., 2002). Calculations of optical properties of aerosols assume internal mixing (Fast et al., 2006), including the Kappa-based hygroscopic growth of aerosol components (Petters and Kreidenweis, 2007). The Rapid Radiative Transfer Model for General Circulation Model schemes (Iacono et al., 2008) is used for shortwave and longwave radiation calculations (Zhao et al., 2011). Other main physical packages used in this study are the Thompson cloud microphysics (Thompson et al., 2008), the Zhang–McFarlane cumulus parameterization (Zhang and McFarlane, 1995), the Mellor–Yamada–Janjic BL scheme (Janjic, 1994), and the Rapid Update Cycle land surface model (Benjamin et al., 2004).

## Radiative and thermodynamic responses to aerosol

Y. Feng et al.

[Title Page](#)[Abstract](#)[Introduction](#)[Conclusions](#)[References](#)[Tables](#)[Figures](#)[Back](#)[Close](#)[Full Screen / Esc](#)[Printer-friendly Version](#)[Interactive Discussion](#)



**Radiative and  
thermodynamic  
responses to aerosol**

Y. Feng et al.

Title Page

Abstract

Introduction

Conclusions

References

Tables

Figures



Back

Close

Full Screen / Esc

Printer-friendly Version

Interactive Discussion



gion of the northern India. Located at  $\sim 1939$  m a.s.l., this site was frequently near the planetary BL top or in the free troposphere during the experimental period. Ground-based AMF-1 multi-filter rotating shadowband radiometer (MFRSR) measurements were made from September 2011 to March 2012. The post-processed, quality-assured AOD products (pghmfrsraod1michM1.s1) from the MFRSR are used to evaluate the model simulations of monthly and daily mean daytime (06:00–18:00 LT) AODs. Instrumental uncertainty in the MFRSR-retrieved AOD is about 0.026 above 380 nm (Schmid et al., 1999), which is generally below the typical AOD levels observed at this site. Monthly mean AERONET (Holben et al., 1998) level 2 sun photometer AOD data sets that are also used have a reported uncertainty of approximately 0.01 at 500 nm (Eck et al., 1999; Smirnov et al., 2000). Comparisons of the simulated monthly mean AODs with Moderate Resolution Imaging Spectroradiometer (MODIS)/Terra satellite observations (MOD08 Level 3, edition 5; Platnick et al., 2003) are used to evaluate the geographic distribution of AOD.

Vertical profiles of aerosol extinction at 532 nm are retrieved at Nainital from micropulse lidar (MPL) backscatter measurements and MFRSR AOD data for March 2012, according to Kafle and Coulter (2013) and Klett (1981). After exclusion of cloud contamination and missing data, 26 days of MPL-retrieved extinction profiles remain, 25 of which have valid data during the daytime when MFRSR AOD retrievals are available. The 30-min-frequency extinction retrievals are averaged hourly and monthly for model comparison with a vertical resolution of  $\sim 500$  m. Aerosol extinction profiles at 532 nm are also available at a nearby low-elevation site, Kanpur ( $26.5^\circ$  N,  $80.3^\circ$  E, a.s.l. 120 m), from the National Aeronautics and Space Administration's MPL network (MPLNET; Welton et al., 2001). Unlike Nainital, which is located near the BL top, the Kanpur site provides aerosol characteristics close to the surface pollution sources in the Indo-Gangetic Basin. During winter and the pre-monsoon season, this site is often loaded with high concentrations of anthropogenic aerosols mixed with dust from episodic events (Dey and Di Girolamo, 2010). The quality-assured MPLNET level 2 daytime products are available from August 2011 to March 2012 for

**Radiative and  
thermodynamic  
responses to aerosol**

Y. Feng et al.

Title Page

Abstract

Introduction

Conclusions

References

Tables

Figures



Back

Close

Full Screen / Esc

Printer-friendly Version

Interactive Discussion



model comparison. In addition to the ground-based remote sensing data, CALIPSO satellite retrievals of extinction profiles from the Cloud-Aerosol Lidar with Orthogonal Polarization sensor (Winker et al., 2009), version 3, level 2, nighttime products are also used to characterize regional variations in aerosol vertical distribution. Uncertainties associated with these lidar retrievals of aerosol extinction profiles, either space-borne or ground-based, include overlapping corrections near the surface, signal-to-noise ratio in the background (Welton and Campbell, 2002), and propagated errors in AOD measurements (Kafle and Coulter, 2013). The observations of extinction profiles are used mainly to identify and correct systematic bias in the model-simulated monthly mean vertical profiles of aerosols. The aerosol abundances in the column are constrained with column-integrated AOD measurements from MFRSR and MODIS.

### 3 Results

#### 3.1 Aerosol optical depth

The model simulations of monthly mean AOD for March 2012 are compared with the MODIS/Terra satellite observations in Fig. 1. Figure 1a and b shows that predicted AODs are generally lower than MODIS retrievals over most of South Asia, but the geographic pattern of AOD distributions is simulated reasonably well. Local maximum AODs in both model predictions and satellite retrievals indicate that the main aerosol sources are located in northern and southwestern India, though they are associated with different threshold values ( $\sim 0.5$  in MODIS and  $\sim 0.25$  in WRF-Chem). Long-range transport of aerosols by the prevailing northwesterly winds in the Indo-Ganges Valley, also represented in both the model calculations and the MODIS data, results in moderately high AODs over the Bay of Bengal. The northeasterly winds recirculate the aerosols from eastern India over to central India, and further down over to the adjacent Arabian Sea. Low AOD values ( $< 0.1$ ) are predicted by WRF-Chem over most of western India and the adjacent oceans, whereas MODIS has some high values ( $> 0.4$ )

over the sea. These discrepancies could be attributable to episodic dust activities not reproduced by WRF-Chem or to overestimation associated with the MODIS satellite retrievals over highly reflective surfaces such as deserts and clouds.

The degree to which the model-calculated AOD is lower than the MODIS data is shown in Fig. 1c. The figure compares the latitudinal variations in AOD averaged between 60 and 95° E. The default model (control run) calculations of AOD are systematically smaller than the MODIS data (by about a factor of 2), from the Equator northward to 27° N (Latitudes north of 27° N are not shown for the MODIS data, because more than 2/3 of the data are missing). Despite the underestimation in absolute AODs, a gradient in AOD calculated as a function of latitude is similar to the MODIS observations, increasing by about ~ 0.1 AOD every 10° in latitude. In addition, comparison of the calculated daily daytime mean AODs with ground-based GVAX MFRSR measurements at Nainital and AERONET data at nearby Kanpur (~ 390 km southeast; the two sites are marked in Fig. 1b) shows that the discrepancies between the modeled and observed AOD are much smaller at the Nainital site in Fig. 1d. The monthly mean AOD at Nainital is estimated at 0.181 by WRF-Chem – about 22 % lower than the value of 0.232 estimated by MFRSR – and the model-data difference is only 13 % if the outlier on day 27 of the observations is excluded. In contrast, the model's underestimation at Kanpur is about 54 %, which is more close to the zonal-mean differences shown in Fig. 1c. These differences in AOD comparison imply that WRF-Chem tends to underpredict aerosol extinction (whose vertical integral is AOD) at lower elevations (in the BL) more than in the free troposphere over this region, because the Nainital data are more representative of the atmosphere near or above the BL top.

### 3.2 Aerosol extinction profiles

To further evaluate the vertical distribution of calculated aerosol extinctions ( $b_{\text{ext}}$ ), the ground-based MPL retrievals available in March at Nainital and Kanpur, along with CALIPSO satellite retrievals, are used. Figure 2 compares the simulated monthly mean vertical profiles of  $b_{\text{ext}}$  with the observational data sets. Like column-integrated AOD,

## Radiative and thermodynamic responses to aerosol

Y. Feng et al.

Title Page

Abstract

Introduction

Conclusions

References

Tables

Figures



Back

Close

Full Screen / Esc

Printer-friendly Version

Interactive Discussion





**Radiative and  
thermodynamic  
responses to aerosol**

Y. Feng et al.

Title Page

Abstract

Introduction

Conclusions

References

Tables

Figures



Back

Close

Full Screen / Esc

Printer-friendly Version

Interactive Discussion



points to model overestimation, consistent with the other sites. The analysis of extinction profiles confirms model underestimation of column AOD in March and moreover, indicates that the low bias in AOD arises mainly from calculated lower aerosol burden in the lower atmosphere, which leads to an AOD underestimate of  $> 50\%$ , irrespective of location. These differences between the observed and modeled profiles at low altitudes are generally larger than the uncertainties associated with ground-based measurements ( $\sim 40\%$ ). Although the CALIPSO satellite retrievals indicate uncertainties of  $\sim 91$  to  $110\%$ , at the two ground sites their monthly mean values are comparable with the ground-based measurements. This validation provides support to the regional mean comparison with the CALIPSO data here, as no sufficient ground-based measurements are available on the regional scale.

To examine potential impacts on calculated radiative and thermodynamic processes from the underestimation of aerosols, sensitivity model runs are conducted for March 2012 by optimizing matching of the observed aerosol vertical profiles. The calculated aerosol extinctions in the lowest eight model layers (below  $\sim 850$  hPa, at  $1.5$ – $3$  km a.s.l. in the simulated model domain) are increased by a factor of 2 at each time step to reduce the identified low bias. However, there are no independent observations of aerosol absorption vertical profiles to constrain the model. AERONET SSA or the satellite-based absorption AOD retrievals provide constraints for column-integrated absorption properties, but neither of them resolves in altitude. To address this uncertainty, two approaches are tested for adjusting the extinction profiles. In Case I, the calculated scattering and absorption coefficients are increased proportionally, so that the altitude-dependent SSA – the fraction of scattering in total extinction – remains the same as in the control run. This case assumes that the underestimation of AOD is contributed proportionally by both scattering and absorbing aerosol loadings. In Case II, only the calculated aerosol scattering coefficient is increased to compensate for the AOD underpredictions, whereas the absorption coefficient remains the same as in the control run, so that the aerosol SSA is increased. This assumption for example could represent for a case study of the underrepresented hygroscopic growth of aerosol par-



5 estimated mean extinction height  $z_{\alpha}$  for the adjusted extinction profiles in the sensitivity studies is generally lowered by about 10–20%. This also results in better agreement with the CALIPSO-inferred mean extinction heights. In the sections below, radiative and thermodynamic responses to these improved aerosol extinction profiles are discussed.

### 5 3.3 Radiative and surface temperature responses

10 The buildup of aerosols in March plays an important role in modulating the distribution of solar radiation throughout the atmosphere over South Asia. In the control run, the aerosol-induced change in net downward solar radiation at the TOA is estimated at about  $-3 \text{ W m}^{-2}$ , averaged over South Asia (Table 3), suggesting an overall cooling effect. On the other hand, aerosols heat the atmosphere by absorbing incoming solar radiation at  $+6.3 \text{ W m}^{-2}$ . This reduces the net downward radiation at the surface (surface dimming) by  $-9.3 \text{ W m}^{-2}$ . These estimated changes in radiation fluxes not only account for the instantaneous perturbation on radiation by aerosols (aerosol direct radiative forcing), but they also include the effects of rapid responses to aerosols at the land surface and in clouds (semi-direct radiative effects). Because aerosol extinctions (thus AODs) in Cases I and II are increased to the same level, the TOA radiative effects of aerosols are similar for the two cases, a net reduction of about  $-5 \text{ W m}^{-2}$ . However, the distribution of incoming solar (shortwave) radiation in the column is very different between the two cases: the estimated atmospheric absorption is 50% stronger in Case I, leading to a larger negative aerosol forcing at the surface ( $-14.2 \text{ W m}^{-2}$ ) than in Case II ( $-11.7 \text{ W m}^{-2}$ ).

15 20 25 The aerosol impact on the surface air temperature (at 2 m) in the model simulations, linked directly to aerosols' perturbation of the radiation budget, is shown in Fig. 3 as a function of latitude over the land and oceans, respectively. Because the sea surface temperature is fixed, the surface air temperature over the ocean responds little to aerosol surface forcing. The near-surface air temperature responds mainly to aerosol heating and increases in the lower atmosphere over the ocean. Therefore, the largest warming is calculated for Case I. In contrast, the absolute changes in the surface air

## Radiative and thermodynamic responses to aerosol

Y. Feng et al.

Title Page

Abstract

Introduction

Conclusions

References

Tables

Figures



Back

Close

Full Screen / Esc

Printer-friendly Version

Interactive Discussion





over the continental source regions. Since the sea surface temperature is fixed in the simulations, stronger lower-atmosphere thermodynamic responses (indicated by larger heating rates) are estimated over the land than over the ocean for BL and LW process.

Consistent with the atmospheric forcing shown in Table 3, Case I estimates the largest diurnal mean SW heating rate (maximum  $\sim 0.7 \text{ K day}^{-1}$ ) of the three cases, and the SW heating rate in Case II is similar to that for the control run (maximum  $\sim 0.35 \text{ K day}^{-1}$ ). Forced by the same aerosol extinction profiles with the bias correction, the differences in calculated heating rates for individual processes between Case I and Case II are shown in Fig. 4. These results demonstrate the impact of different absorbing aerosol profiles on boundary layer dynamics and cloud microphysics processes. The BL cooling is initiated as a dynamical response to both surface dimming (reduced sensible and latent heat fluxes) and atmospheric heating (enhanced or suppressed vertical mixing, depending on height). Over land, the local maximum cooling due to BL mixing occurs at the height with the largest SW heating; the larger SW heating in Case I also drives stronger BL cooling than in Case II. The LW radiation responds similarly to surface dimming and atmosphere heating, so Case I estimates the largest LW cooling over land. Over the ocean, the LW responses are also affected by cloud microphysics processes (i.e., the subsequent latent heat flux exchanges from cloud condensation and evaporation [Micro]). Because absorbing aerosols tend to stabilize the lower atmosphere and suppress the cloud formation, Case I estimates a smaller Micro heating rate at the cloud condensation level and also a smaller LW heating (cooling) below (above) the cloud layer over the ocean than Case II.

The total aerosol impact on the lower-atmosphere temperature profile is determined by the combined effects of all the heating rates (solid black line in Fig. 4). Over the ocean, the total heating rate is strongly governed by the SW heating. Thus, Case I calculates the most significant atmospheric heating by aerosols, which warms most of the lower atmosphere below 600 hPa. The maximum heating occurs below the level where the SW heating rate peaks, because of compensating LW cooling by lower marine clouds. The heating response is different over land. The calculated total heating rate

## Radiative and thermodynamic responses to aerosol

Y. Feng et al.

Title Page

Abstract

Introduction

Conclusions

References

Tables

Figures



Back

Close

Full Screen / Esc

Printer-friendly Version

Interactive Discussion





land surfaces, the BL height is moderately higher (roughly about 200 m) with aerosols, and these regions correspond to areas where aerosols generally have a warming effect on the near-surface air temperature.

Figure 6 illustrates percent changes due to aerosols in meridional circulation ( $v$ ,  $-\omega$ ) and total precipitable water vapor (background color map) averaged at 60–95° E. These changes are linked closely to anomalies of total heating or cooling in the atmosphere (Fig. 4). At 5–20° N where ocean prevails, atmospheric heating by aerosols results in strengthening of the upward motion in all three model simulations, especially below 700 hPa (Fig. 6a–c). This is accompanied by enhanced large-scale subsidence in the lower troposphere north of 20° N where land surface prevails and aerosols have an overall cooling effect due to strong negative LW and BL responses. The largest enhancement in the ascending zone for aerosols is in Case I, which also has the highest absorbing aerosol content. Similarly, Case II, with the strongest cooling, calculates the largest enhancement in the descending zone.

The changes in updraft and downdraft are consistent with the aerosol-induced changes in surface pressure, as illustrated in Fig. 6d for Case I. The decreased pressure over the ocean and an increase over the northern Indian subcontinent are accompanied by enhanced convergence at 850 hPa over the Arabian Sea and enhanced divergence over the eastern India coast, adjacent to the Bay of Bengal. The high-pressure system and divergence drive recirculation of the subsidence flow northward and form more terrain-elevated convection along the Himalayan foothills. Aerosols transported over high-elevation mountains induce a warming effect over the snow-covered surface by reducing the surface albedo, thus enhancing convective updraft over the Qinghai–Tibet Plateau.

In response to the radiative and dynamical perturbation, the aerosol-induced thermodynamic responses are manifested through enhanced surface evaporation and upward transport of clean, moist marine air from the northern Indian Ocean (Fig. 6a–c). The elevation of water vapor to the upper troposphere in the tropics leads to reduced moisture in the middle troposphere over the subtropics. The calculated percent changes

## Radiative and thermodynamic responses to aerosol

Y. Feng et al.

Title Page

Abstract

Introduction

Conclusions

References

Tables

Figures



Back

Close

Full Screen / Esc

Printer-friendly Version

Interactive Discussion







**Radiative and  
thermodynamic  
responses to aerosol**

Y. Feng et al.

Title Page

Abstract

Introduction

Conclusions

References

Tables

Figures



Back

Close

Full Screen / Esc

Printer-friendly Version

Interactive Discussion



trievals of column AOD. Above  $\sim 2$  km, the model's low bias in calculated aerosol extinction is smaller and the extent of the model underestimation also varies depending on the geographical locations. Previous studies have indicated similar low bias (to different extents) in modeled column AOD (Ganguly et al., 2009; Cherian et al., 2013; Pan et al., 2014) and lower-atmosphere extinction coefficients (Yu et al., 2010; Koffi et al., 2012) over this region. Therefore, although the atmospheric radiative and dynamical responses derived from the sensitivity studies in this study are based on the WRF-Chem model used in this study, the dependence on aerosol extinction profiles might also be applicable to other model simulations.

Resolving the mismatch between simulated and observed aerosol extinction profiles requires possible upgrades of multiple model physics schemes, as well as additional high-quality measurements at different locations, and is recommended for future studies over this region. Here, instead of speculating on factors that contribute to the model-data differences, we apply a bias correction to simulated aerosol extinction profiles and demonstrate the impact on regional climate simulations. In our sensitivity studies, increases in aerosol extinction below 2–3 km lead to improved agreement in column AOD, from an underestimation of  $-66$  to  $-11$  % relative to MODIS retrievals averaged over South Asia. This suggests that about 83 % of the AOD underestimation is attributable to model levels below 2–3 km. In addition, the column-mean differences between modeled and CALIPSO extinction profiles averaged over the South Asia domain are reduced from 75 to 40 or 16 % if the CALIPSO profiles are normalized to the MODIS AOD retrievals. In the aerosol-concentrated lower atmosphere below 2–3 km, the predicted regional-mean extinction profile agrees with the CALIPSO retrieval within 30 or 0.4 % compared with the CALIPSO profile normalized to the MODIS AOD.

Compared to the control run, the increased aerosol extinctions in Case I and Case II result in 63 and 80 % larger negative forcing at the TOA for  $-4.9$  and  $-5.4 \text{ W m}^{-2}$ , respectively, and 53 and 26 % stronger dimming effects at the surface for  $-14.2$  and  $-11.7 \text{ W m}^{-2}$ , respectively. The contrast between Case I and Case II demonstrates the importance of constraining the vertical distribution of aerosol absorption, in addition to



**Radiative and  
thermodynamic  
responses to aerosol**

Y. Feng et al.

Title Page

Abstract

Introduction

Conclusions

References

Tables

Figures



Back

Close

Full Screen / Esc

Printer-friendly Version

Interactive Discussion



the climate response to uncertainties in modeled aerosols. In addition, observational constraints on aerosol absorption profiles are lacking. In particular, light absorption by brown carbon aerosols from biomass burning, which are important aerosol sources in South Asia, might contribute additional aerosol absorption (Feng et al., 2013). This absorption enhancement is not considered in this version of the WRF-Chem model used for this study and evaluated. Also, model simulations of semi-direct aerosol effects depend strongly on the model representation of clouds, which is not examined here; on the other hand, cloud occurrences are generally low over this region during the pre-monsoon month.

Nevertheless, this study improves the understanding of model underestimation of aerosols in particular their vertical distribution over South Asia and highlights the importance of accurate representation of both aerosol extinction and absorption profiles in regional climate simulations. Determining whether aerosol scattering or absorption contributes to the aerosol optical underestimation is critical, because the two sensitivity studies here reveal different responses in predicted large-scale dynamics and in subsequent water vapor and cloud distributions. Additional high-quality, routine measurements of both aerosol extinction and absorption profiles are needed. Furthermore, we show that rapid adjustments in the land surface energy budget and atmospheric dynamics modulate the instantaneous radiative perturbation by aerosols with comparable force and can either amplify or offset the direct aerosol radiative forcing. Our results thus reinforce the need for observational constraints of effective radiative forcing, which includes both direct and semi-direct radiative effects, for quantifying aerosol-radiation interactions, as suggested in the Intergovernmental Panel on Climate Change fifth assessment report (Boucher et al., 2013).

*Acknowledgements.* This work was supported by the U.S. Department of Energy (DOE) as part of the Atmospheric System Research Program. Support for this research was provided to Y. Feng, V. R. Kotamarthi, R. Coulter, and M. Cadetdu by Argonne National Laboratory under U.S. DOE contract DE-AC02-06CH11357. C. Zhao's contribution to this study was supported by the U.S. DOE as part of the Regional and Global Climate Modeling program through contract

## References

- Ban-Weiss, G., Cao, L., Bala, G., and Caldeira, K.: Dependence of climate forcing and response on the altitude of black carbon aerosols, *Clim. Dynam.*, 38, 897–911, 2012.
- Benjamin, S. G., Grell, G. A., Brown, J. M., and Smirnova, T. G.: Mesoscale weather prediction with the RUC hybrid isentropic-terrain-following coordinate model, *Mon. Weather Rev.*, 132, 473–494, 2004.
- Bollasina, M. A., Ming, Y., and Ramaswamy, V.: Anthropogenic aerosols and the weakening of the South Asian summer monsoon, *Science*, 334, 502–505, doi:10.1126/science.1204994, 2011.
- Bollasina, M. A., Ming, Y., Ramaswamy, V., Schwarzkopf, M. D., and Naik, V.: Contribution of local and remote anthropogenic aerosols to the twentieth century weakening of the South Asian Monsoon, *Geophys. Res. Lett.*, 41, 680–687, doi:10.1002/2013GL058183, 2014.
- Boucher, O., Randall, D., Artaxo, P., Bretherton, C., Feingold, G., Forster, P., Kerminen, V.-M., Kondo, Y., Liao, H., Lohmann, U., Rasch, P., Satheesh, S. K., Sherwood, S., Stevens, B., and Zhang, X. Y.: Clouds and aerosols, in: *Climate Change 2013: the Physical Science Basis. Contribution of Working Group I to the Fifth Assessment Report of the Intergovernmental Panel on Climate Change*, edited by: Stocker, T. F., Qin, D., Plattner, G.-K., Tignor, M., Allen, S. K., Boschung, J., Nauels, A., Xia, Y., Bex, V., and Midgley, P. M., Cambridge University Press, Cambridge, UK, New York, NY, USA, 2013.
- Cherian, R., Venkataraman, C., Quaas, J., and Ramachandran, S.: GCM simulations of anthropogenic aerosol-induced changes in aerosol extinction, atmospheric heating and precipitation over India, *J. Geophys. Res.-Atmos.*, 118, 2938–2955, doi:10.1002/jgrd.50298, 2013.
- Chin, M., Ginoux, P., Kinne, S., Holben, B. N., Duncan, B. N., Martin, R. V., Logan, J. A., Higurashi, A., and Nakajima, T.: Tropospheric aerosol optical thickness from the GOCART model and comparisons with satellite and sunphotometer measurements, *J. Atmos. Sci.*, 59, 461–483, 2002.
- Choi, J.-O. and Chung, C. E.: Sensitivity of aerosol direct radiative forcing to aerosol vertical profile, *Tellus B*, 66, 24376, doi:10.3402/tellusb.v66.24376, 2014.

## Radiative and thermodynamic responses to aerosol

Y. Feng et al.

Title Page

Abstract

Introduction

Conclusions

References

Tables

Figures



Back

Close

Full Screen / Esc

Printer-friendly Version

Interactive Discussion





## Radiative and thermodynamic responses to aerosol

Y. Feng et al.

Title Page

Abstract

Introduction

Conclusions

References

Tables

Figures



Back

Close

Full Screen / Esc

Printer-friendly Version

Interactive Discussion



Ginoux, P., Chin, M., Tegen, I., Prospero, J. M., Holben, B., Dubovik, O., and Lin, S. J.: Sources and distributions of dust aerosols simulated with the GOCART model, *J. Geophys. Res.-Atmos.*, 106, 20255–20273, 2001.

5 Grell, G. A., Peckham, S. E., Schmitz, R., McKeen, S. A., Frost, G., Skamarock, W. C., and Eder, B.: Fully coupled “online” chemistry within the WRF model, *Atmos. Environ.*, 39, 6957–6975, 2005.

Haywood, J. M. and Shine, K. P.: Multi-spectral calculations of the direct radiative forcing of tropospheric sulphate and soot aerosols using a column model, *Q. J. Roy. Meteor. Soc.*, 123, 1907–1930, 1997.

10 Holben, B. N., Eck, T. F., Slutsker, I., Tanre, D., Buis, J. P., Setzer, A., Vermote, E., Reagan, J. A., Kaufman, Y. J., Nakjima, T., Lavenu, F., Jankowiak, I., and Smirnov, A.: AERONET – a federated instrument network and data archive for aerosol characterization, *Remote Sens. Environ.*, 66, 1–16, 1998.

15 Iacono, M. J., Delamere, J. S., Mlawer, E. J., Shephard, M. W., Clough, S. A., and Collins, W. D.: Radiative forcing by long-lived greenhouse gases: calculations with the AER radiative transfer models, *J. Geophys. Res.*, 113, D13103, doi:10.1029/2008JD009944, 2008.

Jacob, D. J., Crawford, J. H., Maring, H., Clarke, A. D., Dibb, J. E., Emmons, L. K., Ferrare, R. A., Hostetler, C. A., Russell, P. B., Singh, H. B., Thompson, A. M., Shaw, G. E., McCauley, E., Pederson, J. R., and Fisher, J. A.: The Arctic Research of the Composition of the Troposphere from Aircraft and Satellites (ARCTAS) mission: design, execution, and first results, *Atmos. Chem. Phys.*, 10, 5191–5212, doi:10.5194/acp-10-5191-2010, 2010.

Janjic, Z. I.: The step-mountain eta coordinate model: further developments of the convection, viscous sublayer, and turbulence closure schemes, *Mon. Weather Rev.*, 122, 927–945, 1994.

20 Kafle, D. N. and Coulter, R. L.: Micropulse lidar derived aerosol optical depth climatology at ARM sites worldwide, *J. Geophys. Res.*, 118, 7293–7308, doi:10.1002/jgrd.50536, 2013.

25 Kinne, S., Schulz, M., Textor, C., Guibert, S., Balkanski, Y., Bauer, S. E., Bernsten, T., Berglen, T. F., Boucher, O., Chin, M., Collins, W., Dentener, F., Diehl, T., Easter, R., Feichter, J., Fillmore, D., Ghan, S., Ginoux, P., Gong, S., Grini, A., Hendricks, J., Herzog, M., Horowitz, L., Isaksen, I., Iversen, T., Kirkevåg, A., Kloster, S., Koch, D., Kristjansson, J. E., Krol, M., Lauer, A., Lamarque, J. F., Lesins, G., Liu, X., Lohmann, U., Montanaro, V., Myhre, G., Penner, J., Pitari, G., Reddy, S., Seland, O., Stier, P., Takemura, T., and Tie, X.: An AeroCom initial assessment – optical properties in aerosol component modules of global models, *Atmos. Chem. Phys.*, 6, 1815–1834, doi:10.5194/acp-6-1815-2006, 2006.

**Radiative and  
thermodynamic  
responses to aerosol**

Y. Feng et al.

Title Page

Abstract

Introduction

Conclusions

References

Tables

Figures



Back

Close

Full Screen / Esc

Printer-friendly Version

Interactive Discussion



- Klett, J. D.: Stable analytical inversion solution for processing lidar returns, *Appl. Optics*, 20, 211–220, 1981.
- Koch, D., Schulz, M., Kinne, S., McNaughton, C., Spackman, J. R., Balkanski, Y., Bauer, S., Berntsen, T., Bond, T. C., Boucher, O., Chin, M., Clarke, A., De Luca, N., Dentener, F., Diehl, T., Dubovik, O., Easter, R., Fahey, D. W., Feichter, J., Fillmore, D., Freitag, S., Ghan, S., Ginoux, P., Gong, S., Horowitz, L., Iversen, T., Kirkevåg, A., Klimont, Z., Kondo, Y., Krol, M., Liu, X., Miller, R., Montanaro, V., Moteki, N., Myhre, G., Penner, J. E., Perlwitz, J., Pitari, G., Reddy, S., Sahu, L., Sakamoto, H., Schuster, G., Schwarz, J. P., Seland, Ø., Stier, P., Takegawa, N., Takemura, T., Textor, C., van Aardenne, J. A., and Zhao, Y.: Evaluation of black carbon estimations in global aerosol models, *Atmos. Chem. Phys.*, 9, 9001–9026, doi:10.5194/acp-9-9001-2009, 2009.
- Koffi, B., Schulz, M., Breon, F. M., Griesfeller, J., Winker, D., Balkanski, Y., Bauer, S., Berntsen, T., Chin, M. A., Collins, W. D., Dentener, F., Diehl, T., Easter, R., Ghan, S., Ginoux, P., Gong, S. L., Horowitz, L. W., Iversen, T., Kirkevåg, A., Koch, D., Krol, M., Myhre, G., Stier, P., and Takemura, T.: Application of the CALIOP layer product to evaluate the vertical distribution of aerosols estimated by global models: Aero-Com phase I results, *J. Geophys. Res.-Atmos.*, 117, D10201, doi:10.1029/2011jd016858, 2012.
- Kuhlmann, J. and Quaas, J.: How can aerosols affect the Asian summer monsoon? Assessment during three consecutive pre-monsoon seasons from CALIPSO satellite data, *Atmos. Chem. Phys.*, 10, 4673–4688, doi:10.5194/acp-10-4673-2010, 2010.
- Kumar, R., Barth, M. C., Pfister, G. G., Naja, M., and Brasseur, G. P.: WRF-Chem simulations of a typical pre-monsoon dust storm in northern India: influences on aerosol optical properties and radiation budget, *Atmos. Chem. Phys.*, 14, 2431–2446, doi:10.5194/acp-14-2431-2014, 2014.
- Lau, K. M., Kim, M. K., and Kim, K. M.: Asian summer monsoon anomalies induced by aerosol direct forcing: the role of the Tibetan Plateau, *Clim. Dynam.*, 26, 855–864, 2006.
- Lau, K.-M., Kim, K.-M., Hsu, C. N., and Holben, B. N.: Possible influences of air pollution, dust and sandstorms on the Indian monsoon, *WMO Bull.*, 58, 22–30, 2009.
- Liao, H. and Seinfeld, J. H.: Effects of clouds on direct aerosol radiative forcing of climate, *J. Geophys. Res.*, 103, 3781–3788, 1998.
- Liu, X., Easter, R. C., Ghan, S. J., Zaveri, R., Rasch, P., Shi, X., Lamarque, J.-F., Gettelman, A., Morrison, H., Vitt, F., Conley, A., Park, S., Neale, R., Hannay, C., Ekman, A. M. L., Hess, P., Mahowald, N., Collins, W., Iacono, M. J., Bretherton, C. S., Flanner, M. G., and

**Radiative and  
thermodynamic  
responses to aerosol**

Y. Feng et al.

Title Page

Abstract

Introduction

Conclusions

References

Tables

Figures



Back

Close

Full Screen / Esc

Printer-friendly Version

Interactive Discussion



Mitchell, D.: Toward a minimal representation of aerosols in climate models: description and evaluation in the Community Atmosphere Model CAM5, *Geosci. Model Dev.*, 5, 709–739, doi:10.5194/gmd-5-709-2012, 2012.

Loeb, N. G. and Su, W. Y.: Direct aerosol radiative forcing uncertainty based on a radiative perturbation analysis, *J. Climate*, 23, 5288–5293, 2010.

Lohmann, U. and Feichter, J.: Can the direct and semi-direct aerosol effect compete with the indirect effect on a global scale?, *Geophys. Res. Lett.*, 28, 159–161, 2001.

Lu, Z., Zhang, Q., and Streets, D. G.: Sulfur dioxide and primary carbonaceous aerosol emissions in China and India, 1996–2010, *Atmos. Chem. Phys.*, 11, 9839–9864, doi:10.5194/acp-11-9839-2011, 2011.

McComiskey, A., Schwartz, S., Schmid, B., Guan, H., Lewis, E., Ricchiazzi, P., and Ogren, J.: Direct aerosol forcing: calculation from observables and sensitivities to inputs, *J. Geophys. Res.*, 113, D09202, doi:10.1029/2007JD009170, 2008.

Meehl, G. A., Arblaster, J. M., and Collins, W. D.: Effects of black carbon aerosols on the Indian monsoon, *J. Climate*, 21, 2869–2882, doi:10.1175/2008JCLI2362.1, 2008.

Misra, A., Tripathi, S. N., Kaul, D. S., and Welton, E. J.: Study of MPLNET-derived aerosol climatology over Kanpur, India, and validation of CALIPSO Level 2 Version 3 backscatter and extinction products, *J. Atmos. Ocean. Tech.*, 29, 1285–1294, 2012.

Moorthy, K. K., Babu, S. S., Manoj, M. R., and Satheesh, S. K.: Buildup of aerosols over the Indian Region, *Geophys. Res. Lett.*, 40, 1011–1014, doi:10.1002/grl.50165, 2013.

Myhre, G., Berglen, T. F., Johnsrud, M., Hoyle, C. R., Berntsen, T. K., Christopher, S. A., Fehy, D. W., Isaksen, I. S. A., Jones, T. A., Kahn, R. A., Loeb, N., Quinn, P., Remer, L., Schwarz, J. P., and Yttri, K. E.: Modelled radiative forcing of the direct aerosol effect with multi-observation evaluation, *Atmos. Chem. Phys.*, 9, 1365–1392, doi:10.5194/acp-9-1365-2009, 2009.

Myhre, G., Samset, B. H., Schulz, M., Balkanski, Y., Bauer, S., Berntsen, T. K., Bian, H., Bellouin, N., Chin, M., Diehl, T., Easter, R. C., Feichter, J., Ghan, S. J., Hauglustaine, D., Iversen, T., Kinne, S., Kirkevåg, A., Lamarque, J.-F., Lin, G., Liu, X., Lund, M. T., Luo, G., Ma, X., van Noije, T., Penner, J. E., Rasch, P. J., Ruiz, A., Seland, Ø., Skeie, R. B., Stier, P., Takemura, T., Tsigaridis, K., Wang, P., Wang, Z., Xu, L., Yu, H., Yu, F., Yoon, J.-H., Zhang, K., Zhang, H., and Zhou, C.: Radiative forcing of the direct aerosol effect from AeroCom Phase II simulations, *Atmos. Chem. Phys.*, 13, 1853–1877, doi:10.5194/acp-13-1853-2013, 2013.

## Radiative and thermodynamic responses to aerosol

Y. Feng et al.

Title Page

Abstract

Introduction

Conclusions

References

Tables

Figures



Back

Close

Full Screen / Esc

Printer-friendly Version

Interactive Discussion



- Nair, V. S., Solmon, F., Giorgi, F., Mariotti, L., Babu, S. S., and Moorthy, K. K.: Simulation of South Asian aerosols for regional climate studies, *J. Geophys. Res.*, 117, D04209, doi:10.1029/2011JD016711, 2012.
- Pan, X., Chin, M., Gautam, R., Bian, H., Kim, D., Colarco, P. R., Diehl, T. L., Takemura, T., Pozzoli, L., Tsigaridis, K., Bauer, S., and Bellouin, N.: A multi-model evaluation of aerosols over South Asia: common problems and possible causes, *Atmos. Chem. Phys.*, 15, 5903–5928, doi:10.5194/acp-15-5903-2015, 2015.
- Penner, J. E., Zhang, S. Y., and Chuang, C. C.: Soot and smoke aerosol may not warm climate, *J. Geophys. Res.*, 108, 4657, doi:10.1029/2003JD003409, 2003.
- Petters, M. D. and Kreidenweis, S. M.: A single parameter representation of hygroscopic growth and cloud condensation nucleus activity, *Atmos. Chem. Phys.*, 7, 1961–1971, doi:10.5194/acp-7-1961-2007, 2007.
- Pfister, G. G., Parrish, D. D., Worden, H., Emmons, L. K., Edwards, D. P., Wiedinmyer, C., Diskin, G. S., Huey, G., Oltmans, S. J., Thouret, V., Weinheimer, A., and Wisthaler, A.: Characterizing summertime chemical boundary conditions for air masses entering the US West Coast, *Atmos. Chem. Phys.*, 11, 1769–1790, doi:10.5194/acp-11-1769-2011, 2011.
- Platnick, S., King, M. D., Ackerman, S. A., Menzel, W. P., Baum, B. A., Riedi, J. C., and Frey, R. A.: The MODIS cloud products: algorithms and examples from Terra, *IEEE T. Geosci. Remote*, 41, 459–473, 2003.
- Ramana, M. V., Ramanathan, V., Kim, D., Roberts, G. C., and Corrigan, C. E.: Albedo: atmospheric solar absorption and heating rate measurements with stacked UAVs, *Q. J. Roy. Meteor. Soc.*, 133, 1913–1931, 2007.
- Ramanathan, V., Crutzen, P. J., Lelieveld, J., Mitra, A. P., Althausen, D., Anderson, J., Andreae, M. O., Cantrell, W., Cass, G. R., Chung, C. E., Clarke, A. D., Coakley, J. A., Collins, W. D., Conant, W. C., Dulac, F., Heintzenberg, J., Heymsfield, A. J., Holben, B., Howell, S., Hudson, J., Jayaraman, A., Kiehl, J. T., Krishnamurti, T. N., Lubin, D., McFarquhar, G., Novakov, T., Ogren, J. A., Podgorny, I. A., Prather, K., Priestley, K., Prospero, J. M., Quinn, P. K., Rajeev, K., Rasch, P., Rupert, S., Sadourny, R., Satheesh, S. K., Shaw, G. E., Sheridan, P., and Valero, F. P. J.: Indian Ocean experiment: an integrated analysis of the climate forcing and effects of the great Indo-Asian haze, *J. Geophys. Res.*, 106, 28371–28398, 2001.
- Ramanathan, V., Chung, C., Kim, D., Bettge, T., Buja, L., Kiehl, J. T., Washington, W. M., Fu, Q., Sikka, D. R., and Wild, M.: Atmospheric brown clouds: impacts on South Asian climate and hydrological cycle, *P. Natl. Acad. Sci. USA*, 102, 5326–5333, 2005.

## Radiative and thermodynamic responses to aerosol

Y. Feng et al.

Title Page

Abstract

Introduction

Conclusions

References

Tables

Figures



Back

Close

Full Screen / Esc

Printer-friendly Version

Interactive Discussion



Ramanathan, V., Ramana, M. V., Roberts, G., Kim, D., Corrigan, C., Chung, C., and Winker, D.: Warming trends in Asia amplified by brown cloud solar absorption, *Nature*, 448, 575–578, doi:10.1038/nature06019, 2007.

5 Samset, B. H., Myhre, G., Schulz, M., Balkanski, Y., Bauer, S., Berntsen, T. K., Bian, H., Belouin, N., Diehl, T., Easter, R. C., Ghan, S. J., Iversen, T., Kinne, S., Kirkevåg, A., Lamarque, J.-F., Lin, G., Liu, X., Penner, J. E., Seland, Ø., Skeie, R. B., Stier, P., Takemura, T., Tsigaridis, K., and Zhang, K.: Black carbon vertical profiles strongly affect its radiative forcing uncertainty, *Atmos. Chem. Phys.*, 13, 2423–2434, doi:10.5194/acp-13-2423-2013, 2013.

10 Satheesh, S. K., Moorthy, K. K., Babu, S. S., Vinoj, V., and Dutt, C. B. S.: Climate implications of large warming by elevated aerosol over India, *Geophys. Res. Lett.*, 35, L19809, doi:10.1029/2008GL034944, 2008.

15 Satheesh, S. K., Moorthy, K. K., Babu, S. S., Vinoj, V., Nair, V. S., Beegum, S. N., Dutt, C. B. S., Alappattu, D. P., and Kunhikrishnan, P. K.: Vertical structure and horizontal gradients of aerosol extinction coefficients over coastal India inferred from airborne lidar measurements during the Integrated Campaign for Aerosol, Gases and Radiation Budget (ICARB) field campaign, *J. Geophys. Res.*, 114, D05204, doi:10.1029/2008JD011033, 2009.

Schmid, B., Michalsky, J., Halthore, R., Beauharnois, M., Harrison, L., Livingston, J., Russell, P., Holben, B., Eck, T., and Smirnov, A.: Comparison of aerosol optical depth from four solar radiometers during the fall 1997 ARM intensive observation period, *Geophys. Res. Lett.*, 26, 2725–2728, doi:10.1029/1999GL900513, 1999.

20 Schwarz, J. P., Spackman, J. R., Gao, R. S., Watts, L. A., Stier, P., Schulz, M., Davis, S. M., Wofsy, S. C., and Fahey, D. W.: Global-scale black carbon profiles observed in the remote atmosphere and compared to models, *Geophys. Res. Lett.*, 37, L18812, doi:10.1029/2010GL044372, 2010.

25 Shindell, D. T., Lamarque, J.-F., Schulz, M., Flanner, M., Jiao, C., Chin, M., Young, P. J., Lee, Y. H., Rotstain, L., Mahowald, N., Milly, G., Faluvegi, G., Balkanski, Y., Collins, W. J., Conley, A. J., Dalsoren, S., Easter, R., Ghan, S., Horowitz, L., Liu, X., Myhre, G., Nagashima, T., Naik, V., Rumbold, S. T., Skeie, R., Sudo, K., Szopa, S., Takemura, T., Voulgarakis, A., Yoon, J.-H., and Lo, F.: Radiative forcing in the ACCMIP historical and future climate simulations, *Atmos. Chem. Phys.*, 13, 2939–2974, doi:10.5194/acp-13-2939-2013, 2013.

30 Skamarock, W. C., Klemp, J. B., Dudhia, J., Gill, D. O., Barker, D. M., Wang, W., and Powers, J. G.: A description of the advanced research WRF version 2, NCAR Tech. Note,

**Radiative and  
thermodynamic  
responses to aerosol**

Y. Feng et al.

Title Page

Abstract

Introduction

Conclusions

References

Tables

Figures



Back

Close

Full Screen / Esc

Printer-friendly Version

Interactive Discussion



NCAR/TN-468+STR, Natl. Cent. for Atmos. Res., Boulder, Colo, available at: <http://www2.mmm.ucar.edu/wrf/users/pub-doc.html> (last access: 16 June 2015), 2008.

Smirnov, A., Holben, B. N., Eck, T. F., Dubovik, O., and Slutsker, I.: Cloud screening and quality control algorithms for the AERONET data base, *Remote Sens. Environ.*, 73, 337–349, 2000.

Thompson, G., Field, P. R., Rasmussen, R. M., and Hall, W. D.: Explicit forecasts of winter precipitation using an improved bulk microphysics scheme. Part II: Implementation of a new snow parameterization, *Mon. Weather Rev.*, 136, 5095–5115, 2008.

Vuolo, M. R., Schulz, M., Balkanski, Y., and Takemura, T.: A new method for evaluating the impact of vertical distribution on aerosol radiative forcing in general circulation models, *Atmos. Chem. Phys.*, 14, 877–897, doi:10.5194/acp-14-877-2014, 2014.

Wang, C., Kim, D., Ekman, A. M. L., Barth, M. C., and Rasch, P. J.: Impact of anthropogenic aerosols on Indian summer monsoon, *Geophys. Res. Lett.*, 36, L21704, doi:10.1029/2009GL040114, 2009.

Welton, E. J. and Campbell, J. R.: Micropulse lidar signals: uncertainty analysis, *J. Atmos. Ocean. Tech.*, 19, 2089–2094, 2002.

Welton, E. J., Campbell, J. R., Spinhirne, J. D., and Scott III, V. S.: Global monitoring of clouds and aerosols using a network of micropulse lidar systems, *SPIE Proc. Ser.*, 4153, 151–158, doi:10.1117/12.417040, 2001.

Winker, D. M., Vaughan, M. A., Omar, A. H., Hu, Y., Powell, K. A., Liu, Z., Hunt, W. H., and Young, S. A.: Overview of the CALIPSO mission and CALIOP data processing algorithms, *J. Atmos. Ocean. Tech.*, 26, 2310–2323, 2009.

Yevich, R. and Logan, J. A.: An assessment of biofuel use and burning of agricultural waste in the developing world, *Global Biogeochem. Cy.*, 17, 1095, doi:10.1029/2002GB001952, 2003.

Yu, H., Dickinson, R. E., Chin, M., Kaufman, Y. J., Holben, B. N., Geogdzhayev, I. V., and Mishchenko, M. I.: Annual cycle of global distributions of aerosol optical depth from integration of MODIS retrievals and GOCART model simulations, *J. Geophys. Res.*, 108, 4128, doi:10.1029/2002JD002717, 2003.

Yu, H. B., Chin, M., Winker, D. M., Omar, A. H., Liu, Z. Y., Kittaka, C., and Diehl, T.: Global view of aerosol vertical distributions from CALIPSO lidar measurements and GOCART simulations: regional and seasonal variations, *J. Geophys. Res.*, 115, D00H30, doi:10.1029/2009JD013364, 2010.

Zarzycki, C. M. and Bond, T. C.: How much can the vertical distribution of black carbon affect its global direct radiative forcing?, *Geophys. Res. Lett.*, 37, L20807, doi:10.1029/2010gl044555, 2010.

Zhang, G. J. and McFarlane, N. A.: Sensitivity of climate simulations to the parameterization of cumulus convection in the Canadian Climate Centre general circulation model, *Atmos. Ocean*, 33, 407–446, 1995.

Zhao, C., Liu, X., Ruby Leung, L., and Hagos, S.: Radiative impact of mineral dust on monsoon precipitation variability over West Africa, *Atmos. Chem. Phys.*, 11, 1879–1893, doi:10.5194/acp-11-1879-2011, 2011.

**Radiative and thermodynamic responses to aerosol**

Y. Feng et al.

Title Page

Abstract

Introduction

Conclusions

References

Tables

Figures



Back

Close

Full Screen / Esc

Printer-friendly Version

Interactive Discussion



## Radiative and thermodynamic responses to aerosol

Y. Feng et al.

**Table 1.** Estimated differences relative to CALIPSO extinction profiles at Nainital, Kanpur, and South Asia in March 2012.

Site	Column Differences (%)			Differences below 850 hPa (%)		
	Model (control run)	Model (increased extinction)	Model (increased extinction)*	Model (control run)	Model (increased extinction)	Model (increased extinction)*
Nainital	–33	–22	–25	–56	–12	–16
Kanpur	–33	–14	–33	–52	–11	–31
S. Asia	–75	–40	–16	–77	–30	–0.4

\* Percent differences relative to the CALIPSO extinction profiles normalized to the column AOD inferred from the surface measurements for Nainital and Kanpur and the MODIS data for South Asia.

Title Page

Abstract

Introduction

Conclusions

References

Tables

Figures



Back

Close

Full Screen / Esc

Printer-friendly Version

Interactive Discussion







## Radiative and thermodynamic responses to aerosol

Y. Feng et al.

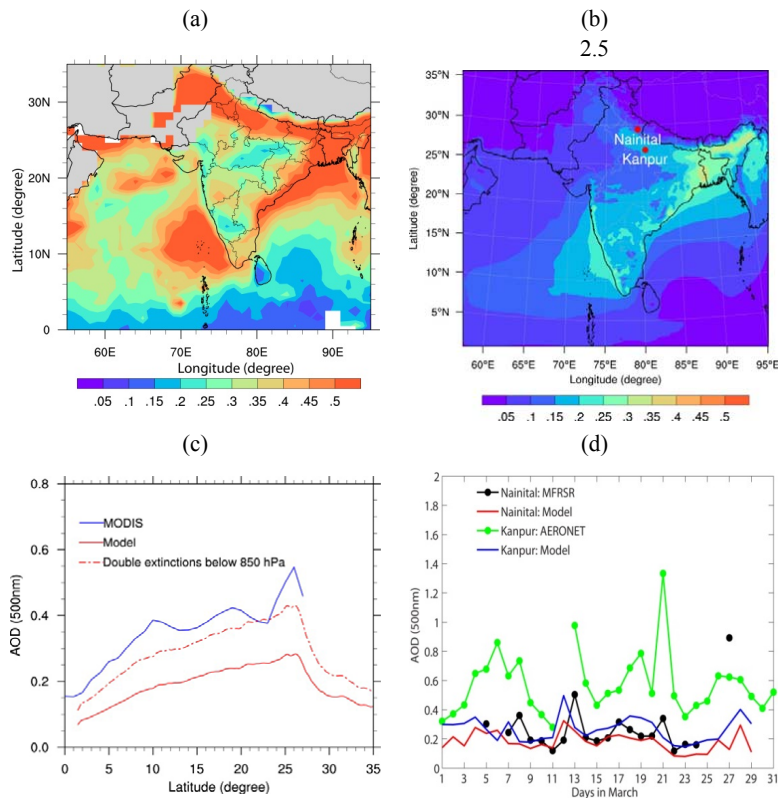


**Figure 1.** For March 2012: **(a)** MODIS-retrieved and **(b)** simulated monthly mean AOD distributions over South Asia. The locations of Nainital and Kanpur sites are indicated by red dots. **(c)** Latitudinal variations in AOD averaged for 60–95° E from the model control run (red solid), sensitivity runs (red dotted dash), and MODIS retrievals (blue). North of 27° N, more than 2/3 of the MODIS AODs are missing (data not shown). **(d)** Comparison of simulated and observed daily mean AOD at Nainital and Kanpur.

Title Page

Abstract

Introduction

Conclusions

References

Tables

Figures



Back

Close

Full Screen / Esc

Printer-friendly Version

Interactive Discussion

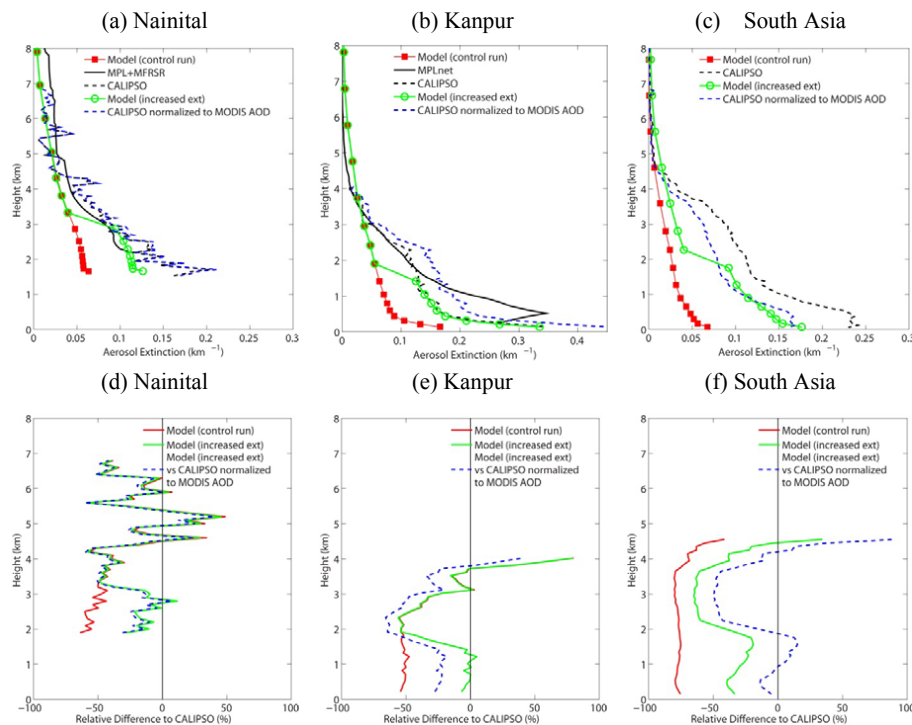


**Figure 2.** Comparisons of monthly mean aerosol extinction profiles from model calculations at 550 nm (red squares for the control run and green open circles for the sensitivity studies), ground-based MPL data at 532 nm (solid black), satellite-retrieved CALIPSO data at 532 nm (dashed black), and CALIPSO data normalized to the MODIS AODs (dashed blue) **(a)** at Nainital, **(b)** at Kanpur, and **(c)** over South Asia (60–95° E, 0–30° N), respectively. The column-mean uncertainty in CALIPSO extinction data is  $\pm 110$ ,  $\pm 93$ , and  $\pm 91$  % in **(a–c)**; Percent differences between the simulated and CALIPSO profiles are shown for **(d)** Nainital, **(e)** Kanpur, and **(f)** South Asia.

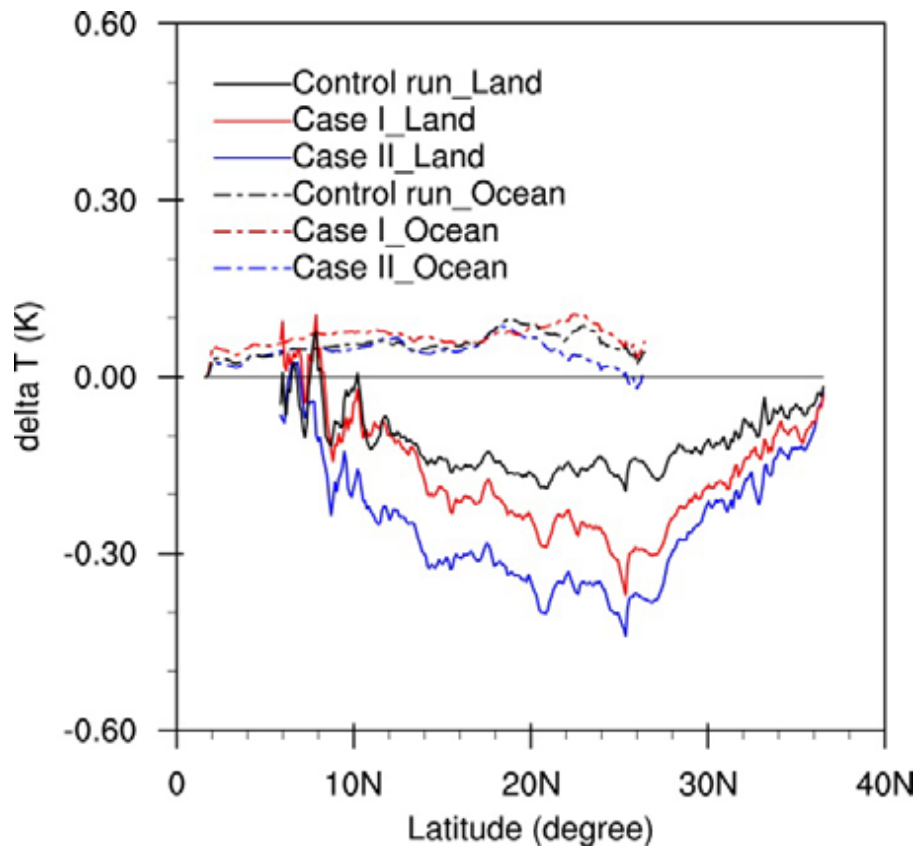


**Figure 3.** Changes in surface air temperature (K) due to aerosol radiative effects for three model simulations.

**Radiative and thermodynamic responses to aerosol**

Y. Feng et al.

Title Page	
Abstract	Introduction
Conclusions	References
Tables	Figures
◀	▶
◀	▶
Back	Close
Full Screen / Esc	
Printer-friendly Version	
Interactive Discussion	



## Radiative and thermodynamic responses to aerosol

Y. Feng et al.

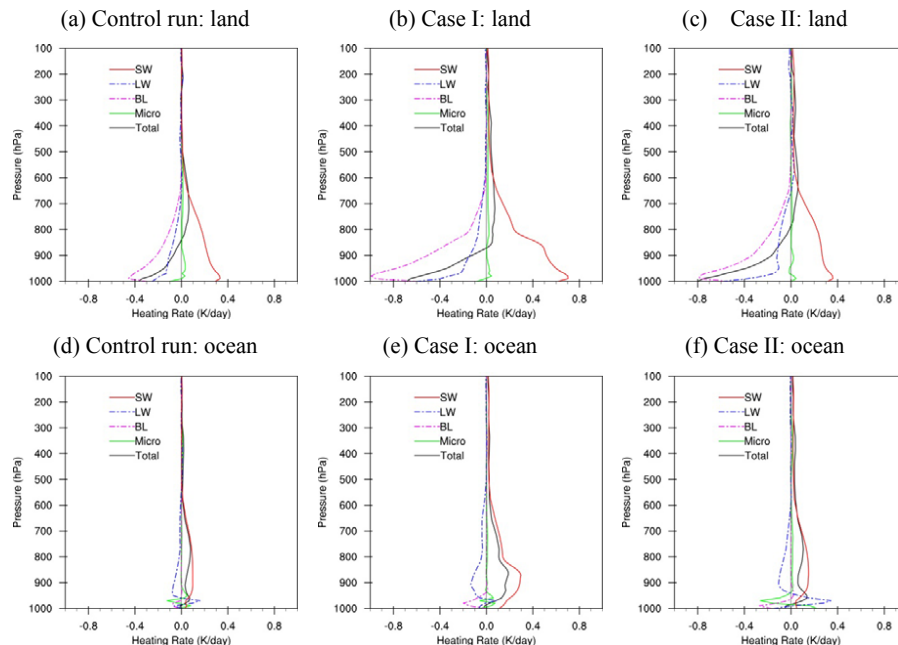


**Figure 4.** Calculated monthly mean heating rates (temperature tendency,  $dT/dt$ , in  $\text{K day}^{-1}$ ) perturbed by aerosols, over land for (a) the control run, (b) Case I, and (c) Case II, as well as over the ocean for (d) the control run, (e) Case I, and (f) Case II. The heating processes include shortwave (SW) radiation (red), longwave (LW) radiation (blue dashed), boundary mixing (BL; magenta dashed), and cloud microphysics (Micro; green). The total heating due to aerosol effects is shown with solid black lines.

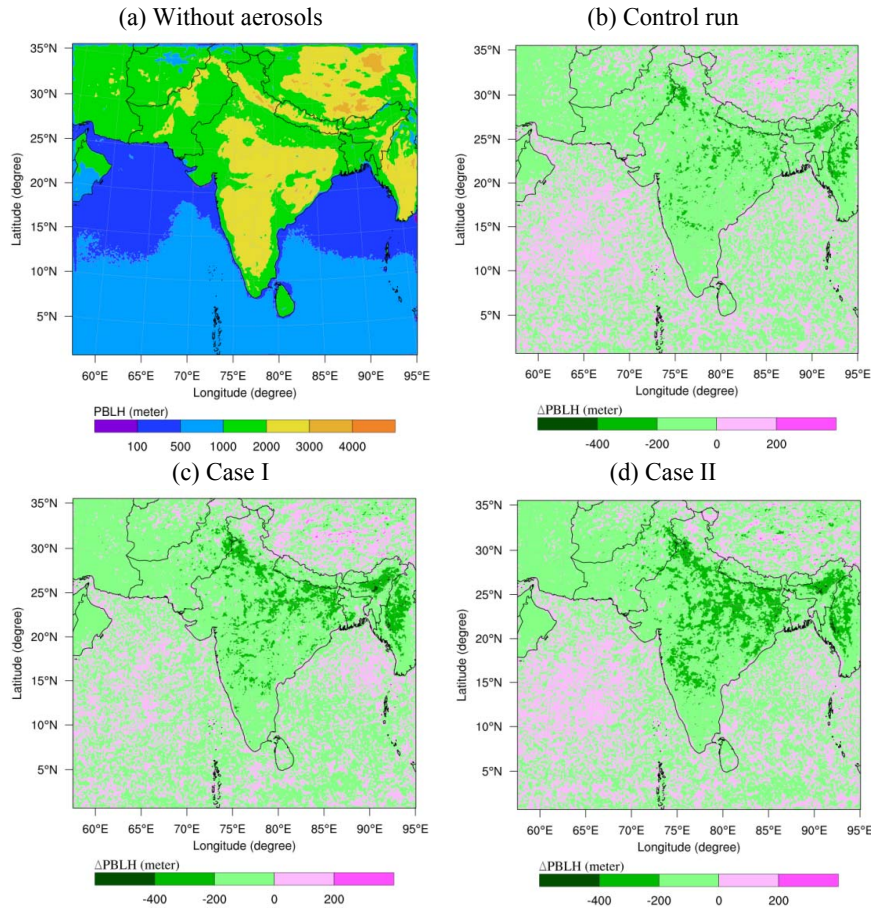


**Figure 5.** (a) Calculated monthly mean planetary BL height (PBLH) at 13:00–14:00LT for March, without aerosols; and estimated changes in PBLH ( $\Delta$ PBLH) due to aerosols in (b) the control run, (c) Case I, and (d) Case II.

Radiative and  
thermodynamic  
responses to aerosol

Y. Feng et al.

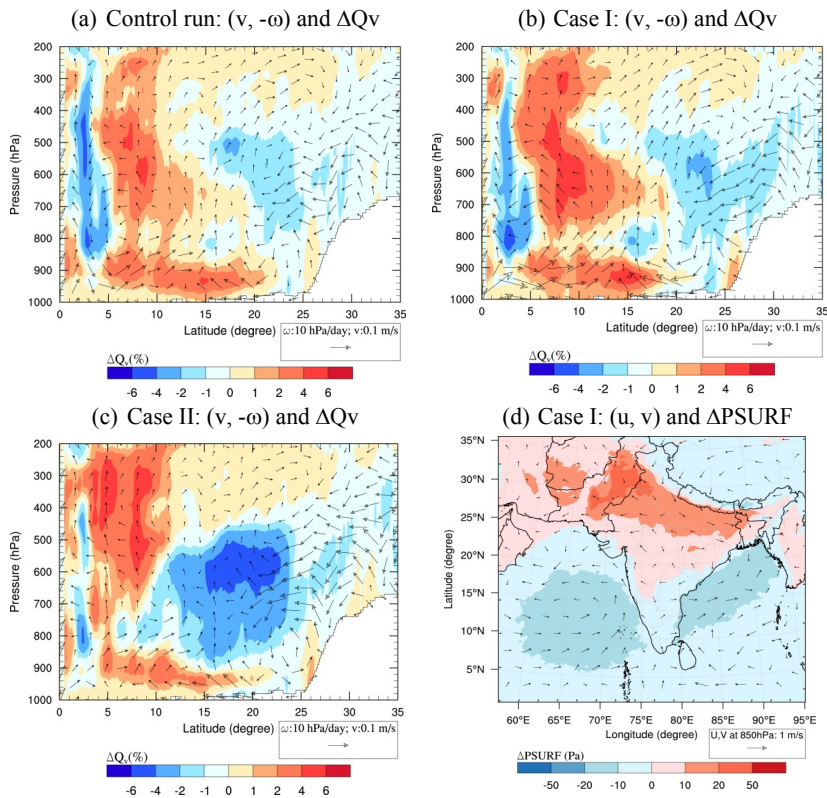


**Figure 6.** Changes in meridional circulation ( $v$ ,  $-\omega$ ), averaged at 60–95° E, due to different aerosol effects for (a) the control run, (b) Case I, and (c) Case II, where  $v$  (scaled to  $0.1 \text{ m s}^{-1}$ ) is the meridional velocity, and  $-\omega$  (scaled to  $10 \text{ hPa day}^{-1}$ ) is the vertical velocity. The color-shaded contours in the background indicate the changes (%) in total precipitable water ( $\Delta Q_v$ ) in the column due to aerosols. Panel (d) shows the changes in horizontal winds ( $u$ ,  $v$ ) at 850 hPa and surface pressure changes ( $\Delta PSURF$ ) due to aerosols for Case I.

Radiative and  
thermodynamic  
responses to aerosol

Y. Feng et al.

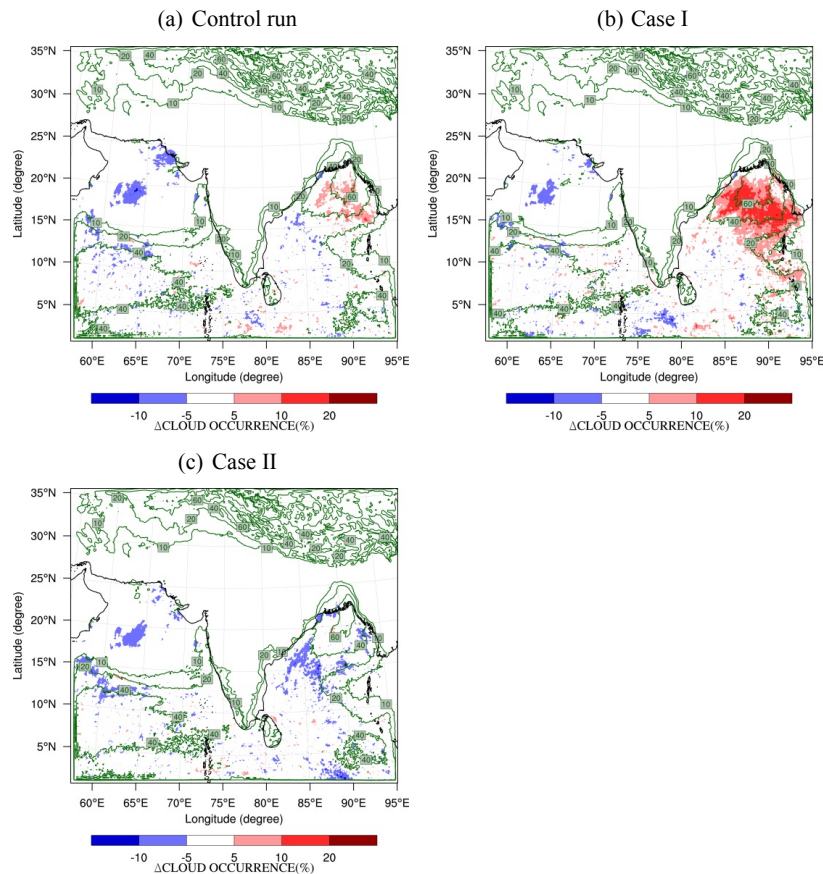


**Figure 7.** Changes in frequency of cloud occurrence (defined as % of hours in a month with clouds below 500 hPa in each column) due to aerosols for **(a)** the control run, **(b)** Case I, and **(c)** Case II. The contour lines in green color in each panel indicate calculated frequency of cloud occurrence without aerosols. The contour levels are shown for 10, 20, 40, and 60 %.

Title Page

Abstract

Introduction

Conclusions

References

Tables

Figures



Back

Close

Full Screen / Esc

Printer-friendly Version

Interactive Discussion

